Conference Proceedings

EuroSun 2014
Aix-les-Bains (France), 16 – 19 September 2014

Comparison of different modeling methods for a single effect water-lithium bromide absorption chiller

François Boudéhenn[1], Sylvain Bonnot[1], Hélène Demasles[1] and Amine Lazrak[1]

[1] CEA LITEN INES, Le Bourget du Lac (France)

Abstract

This paper presents a comparison of different absorption chiller modeling methods. Models were validated using experimental data of a single effect water-lithium bromide absorption chiller. Six of the models considered are empirically based ones and the last considered model is a physical one (PhM). The empirical modeling methods compared are: the adapted Gordon-Ng model (GNA), the characteristic equation model ($\Delta\Delta T$) and the adapted characteristic equation model ($\Delta\Delta T'$), the multivariable polynomial model (MPR), the artificial neural network model (ANN) and the Carnot function model (CFM). These models are used to predict the effects of external water operating condition on cooling capacity (Q_E) and thermal COP (COP_{th}). Models parameters are calculated using a constant methodology and accuracy evaluation of each model is done in the paper through comparisons between numerical and experimental results.

Key-words: absorption chiller, modeling methods, experimental and numerical results comparison

1. Introduction

For several years, absorption chiller numerical models have been presented in the literature this is why complete review of them will not be presented in this paper. Among these numerical models, some are empirically based ones, others are physical ones. The choice of a numerical model can be linked to the precision of the numerical results, the complexity to incorporate it into simulation software, the number of parameters to identify, the calculation time etc. Most of the time, only the external operating conditions are known and the available number of experimental points (or manufacturer catalog data), required to identify the parameters, is insufficient.

From these observations, this paper aims to compare several absorption chiller modeling methods. The models will be empirically or physically based model. Each one will need a set of parameters that will be identified using the same methodology and a first set of experimental data in steady state conditions. The comparison between models will then be done on the second set of experimental data.

In this paper six empirically based models and one physically based model are compared. Among the empirically based models, four are well-known methods and are well-described by Labus et al. (2013). The original characteristic temperature function method was proposed first by Ziegler et al. (1999). The last empirically based model (CFM) is shortly described by Le Denn et al. (2013) and will be more detailed in this paper. The physically based model is based on thermodynamic description of absorption chillers by Herold et al. (1996). Before the different modeling methods descriptions, the absorption chiller and the experimental data will be presented. Finally a comparison between numerical and experimental results is done and an accuracy analysis is proposed.

2. Absorption chiller description and experimental data

The absorption chiller used is a single effect water-lithium bromide chiller manufactured by the German company EAW with a nominal cooling capacity of 15 kW. The nominal thermal COP specified by the

Selection and/or peer review under responsibility of EuroSun2014 Scientific Committee
doi:10.18086/eurosun.2014.07.04 Available at http://proceedings.ises.org

manufacturer (EAW, 2012) is 0.71. The hydraulic specifications of this chiller are presented in Table 1.

Tab. 1: Hydraulic specifications of the 15 kW cooling capacity EAW absorption chiller (EAW, 2012)

EAW Wegracal SE 15	Capacities	Inlet/outlet nominal temperatures	Inlet min/max temperatures	Flowrates	Pressure losses
	[kW]	[°C]	[°C]	[m^3/h]	[mbars]
Evaporator	15	17 / 11	6 / -	1.9	400
Generator	21	90 / 80	70 / 95	1.8	400
Absorber-Condenser	35	30 / 36	25 / 40	5	900

Experimental data required for parameters determination of each model and for its validation have been obtained using a test bench where the chiller was tested in steady-state conditions as part of the AbClimSol project (Boudéhenn et al., 2010), Figure 1. The test bench is equipped with temperature sensors (uncertainty of 0.1K on T and 0.25K on the ΔT) at the inlet and outlet of the tested component and with mass flow rate sensors (uncertainty of 0.2% of the measured value) on each hydraulic loop.

Fig. 1: Picture of the absorption chiller connected to the INES test bench

Amongst the 35 available steady-states points, 15 points were used to identify each model parameters and 20 points for the comparison between numerical and experimental results. Table 2 presents the operating conditions ranges on each water loop connected to the chiller.

Tab. 2: Operating condition ranges during experimental tests on each water loop connected to the chiller

Water loop	**Inlet temperature**		**Outlet temperature**		**Thermal power**	
	Min.	**Max.**	**Min.**	**Max.**	**Min.**	**Max.**
	[°C]	[°C]	[°C]	[°C]	[kW]	[kW]
Evaporator	7.9	23.7	5.9	15.1	4.138	19.369
Generator	69.4	93.6	61.4	84.1	10.558	29.135
Absorber - Condenser	25.0	40.0	29.8	44.7	14.626	49.238

Using the 15 experimental points, parameters identifications of the different models have been done using 'datafit' function in Scilab[1]. The 'datafit' function is a parameters identification method based on a nonlinear regression of measured data.

[1] http://www.scilab.org/

3. Numerical models descriptions

3.1. Adapted Gordon-Ng model

The adapted Gordon-Ng model (GNA) was proposed first by Gordon and Ng (1995) from a general thermodynamic model for cooling devices. According to the authors, the losses due to the finite-rate mass transfer (corresponding to the dominant irreversibility of the absorption chillers) can therefore be approximated as temperature independent. The model was based on the external temperature of the four main heat exchangers. Labus et al. (2013) have modified it to explain it with a single temperature source for the absorber and condenser (eq. 1).

$$\frac{1}{COP_{th}} = \left(\frac{T_{AC}^{in}-T_E^{out}}{T_E^{out}}\right)\cdot\left(\frac{T_G^{in}}{T_G^{in}-T_{AC}^{in}}\right) + \left(\frac{1}{Q_E}\right)\cdot\left(\frac{T_G^{in}}{T_G^{in}-T_{AC}^{in}}\right)\cdot\left(\alpha_1 - \alpha_2\cdot\frac{T_{AC}^{in}}{T_G^{in}}\right) \quad \text{(eq. 1)}$$

According to (eq. 1), the cooling capacity can be expressed by the following equation:

$$Q_E = \frac{\left(\frac{T_G^{in}}{T_G^{in}-T_{AC}^{in}}\right)\cdot\left(\alpha_1-\alpha_2\cdot\frac{T_{AC}^{in}}{T_G^{in}}\right)}{\frac{1}{COP_{th}}-\left[\left(\frac{T_{AC}^{in}-T_E^{out}}{T_E^{out}}\right)\cdot\left(\frac{T_G^{in}}{T_G^{in}-T_{AC}^{in}}\right)\right]} \quad \text{(eq. 2)}$$

In (eq. 1) and (eq. 2), α_1 and α_2 are the two parameters to identify.

3.2. Characteristic temperature function and adapted characteristic temperature function models

Ziegler et al. (1999) have proposed an approximate method which is able to represent the thermal powers (on the three hydraulic loops) as linear functions of a simple equation based on external temperatures. This equation so-called the characteristic temperature function ($\Delta\Delta T$) depends of the average temperature (eq. 3) and supposes that the heat transfer coefficients are constant.

$$\Delta\Delta T = \frac{T_G^{in}+T_G^{out}}{2} + R\cdot\frac{T_E^{in}+T_E^{out}}{2} - (1+R)\cdot\frac{T_{AC}^{in}+T_{AC}^{out}}{2} \quad \text{(eq. 3)}$$

R is the Dühring parameter, function of salt concentration, which can be approximated by a constant value and can be used as a model parameter. Using (eq. 3), thermal power can be expressed as a linear function.

$$Q_X = a_X\cdot\Delta\Delta T + b_X \quad \text{(eq. 4)}$$

In (eq. 4), a_x and b_x are two parameters for thermal load Q_x relative to the hydraulic loop X. So, for the three hydraulic loops (evaporator, generator and absorber-condenser), 6 parameters plus the Dühring one have to be identified.

Khün and Ziegler (2005) have shown that the predicted performance of the cooling capacity (P_E) can deviate considerably from the linear behavior, especially at high driving temperature due to the increase of the internal losses. According to this point, an adapted characteristic temperature function ($\Delta\Delta T'$) model has been proposed according to (eq. 5).

$$\Delta\Delta T' = \frac{T_G^{in}+T_G^{out}}{2} + R_1\cdot\frac{T_E^{in}+T_E^{out}}{2} - R_2\cdot\frac{T_{AC}^{in}+T_{AC}^{out}}{2} \quad \text{(eq. 5)}$$

In (eq. 5), R_1 and R_2 are two parameters to identify, replacing the Dühring parameter. In the same way as previously, the thermal power can be expressed as a linear function according to (eq. 6), where a'_x and b'_x are 2 parameters to identify for each 3 thermal powers.

$$Q_X = a'_X\cdot\Delta\Delta T' + b'_X \quad \text{(eq. 6)}$$

3.3. Multivariable polynomial model

Labus et al. (2013) precise that the multivariable polynomial model (MPR) is a black-box type model, and is very effective to describe complex non-linear relationships between input and output variables, without integrating the physical processes into the model description. The authors present a generalized second order model according to (eq. 7).

$$Q_E = \beta_0^E + \beta_1^E\cdot T_G^{in} + \beta_2^E\cdot T_{AC}^{out} + \beta_3^E\cdot T_E^{in} + \beta_4^E\cdot T_G^{in}\cdot T_{AC}^{out} + \beta_5^E\cdot T_G^{in}\cdot T_E^{in}$$
$$+\beta_6^E\cdot T_{AC}^{out}\cdot T_E^{in} + \beta_7^E\cdot\left(T_G^{in}\right)^2 + \beta_8^E\cdot(T_{AC}^{out})^2 + \beta_9^E\cdot\left(T_E^{in}\right)^2 \quad \text{(eq. 7)}$$

The other thermal powers (Q_G and Q_{AC}) can be described in the same way, with finally 30 parameters to identify for the MPR model. Using Q_E and Q_G, the thermal COP can be expressed by the following equation:

$$COP_{th} = \frac{Q_E}{Q_G} \quad \text{(eq. 8)}$$

3.4. Artificial neural network model

The artificial neural network models (ANN) are inspired from biological neurons and they are related to artificial intelligence. They are black-box type models and, more precisely, they are adaptive systems which can be trained in order to represent a particular behavior as a response to defined inputs. Labus et al. (2013) and Hernandez et al. (2013) have specified that the most common ANN architecture applied to absorption chillers are feed-forward neural networks trained using a back-propagation algorithm. The ANN chosen in this work is a feed-forward neural network with bias and one hidden layer containing 6 neurons. The 3 inputs (vector x) are the linear normalizations of T_{AC}^{in}, T_G^{in} and T_E^{out}. The 2 outputs (vector y) are the linear normalizations of Q_E and COP_{th}. The activation function φ, used in the hidden and output layers, is the sigmoid one (eq. 9).

$$\varphi(X) = \frac{1}{1+e^{-X}} \quad \text{(eq. 9)}$$

The normalization is made in order to include each series from an interval [min; max] (defined in the table 1) to a normalized interval [0,1; 0,9]. The following equations allow calculating outputs y from inputs x, with matrix b and w as parameters:

$$z_{1,k} = \varphi\left(b_{1,k} + \sum_{j=1}^{3} w_{1,k,j} \cdot x_j\right) \quad for\ k = 1\ to\ 6 \quad \text{(eq. 10)}$$

$$y_k = \varphi\left(b_{1,k} + \sum_{j=1}^{6} w_{2,k,j} \cdot z_{1,j}\right) \quad for\ k = 1\ to\ 2 \quad \text{(eq. 11)}$$

Finally, Q_E and COP_{th} are obtained by an inverse normalization of y from the interval [0,1 ; 0,9] to the original interval [min ; max].

Usually 70% of data are used for training, 20% for validation and the last 10% for model testing (Labus et al., 2013). In this study, the ANN was trained with only 40% of data and 60% were used for model testing.

3.5. Carnot function model

The Carnot function model (CFM) is shortly presented by Le Denn et al. (2013). This model is used in the PISTACHE tool in order to calculate the performances of the sorption chiller integrated into a solar cooling and heating plant (Siré et al., 2013 and Semmari et al., 2014). The CFM model is based on the expression of the ideal performances of a thermodynamic machine through the use of the Carnot efficiency. The Carnot efficiency describes the theoretical maximal efficiency, i.e. without any irreversibility, that can be reaching by a thermodynamic cycle. For a sorption chiller, the Carnot efficiency can be expressed as a function of the external temperatures by (eq. 12):

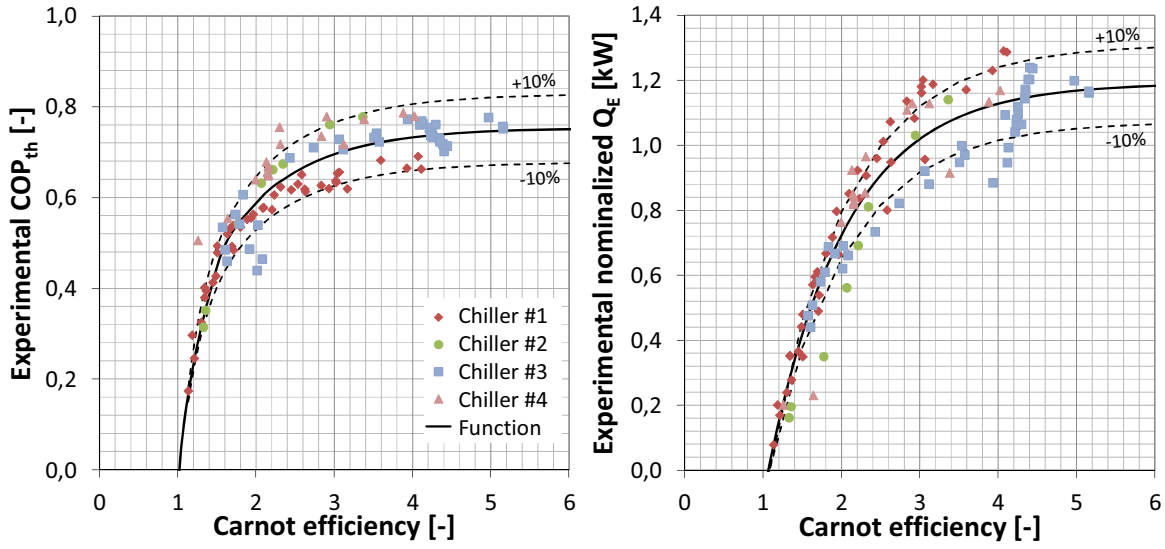

Fig. 2: Experimental COP_{th} (left) and Q_E (right) as functions of the Carnot efficiency for several absorption chillers

$$\eta_{Carnot} = \frac{T_G^{in} - T_{AC}^{in}}{T_{AC}^{in} - T_E^{in}} \cdot \frac{T_E^{in}}{T_G^{in}} \quad \text{(eq. 12)}$$

As presented in Le Denn et al. (2013) and based on the experimental results on several absorption chillers tested on the test bench described previously, the thermal COP and the cooling capacity can be described as a function of the Carnot efficiency (Fig. 2).

The cooling capacity represented on the figure 2 is the normalized one (i.e. experimental cooling capacity divided by the nominal cooling capacity) in order to allow a global representation for the different tested chillers. The generic functions used in the figure 2 are described by the equation 13 for COP_{th} and by the equation 14 for Q_E.

$$COP_{th} = \omega_1 \cdot e^{\left(\frac{-\eta_{Carnot}}{\tau_1}\right)} + \omega_2 \cdot e^{\left(\frac{-\eta_{Carnot}}{\tau_2}\right)} + COP_{th,0} \quad \text{(eq. 13)}$$

$$Q_E = \delta_1 \cdot e^{\left(\frac{-\eta_{Carnot}}{\theta_1}\right)} + \delta_2 \cdot e^{\left(\frac{-\eta_{Carnot}}{\theta_2}\right)} + Q_{E,0} \quad \text{(eq. 14)}$$

With ω_1, τ_1, ω_2, τ_2, $COP_{th,0}$, δ_1, θ_1, δ_2, θ_2 and $Q_{E,0}$, 10 parameters to identify. Of course, the parameters of the generic function can be identified for a single chiller, in order to obtain the maximum accuracy.

3.6. Physical model

The physical model is based on the description made by Herold et al. (1996) through the heat and mass balances on each components of the chiller. The physical properties are available in EES[1] or can be calculated with the correlation given by Schenk (2008) and Lansing (1976).

The four main heat exchangers are modeled using the log mean temperature difference (LMTD) method or the simple mean temperature difference versus the heat and mass balances, respectively described by (eq. 15) to (eq. 20).

$$Q_A = \dot{m}_{AC} \cdot Cp_w \cdot \left(T_{AC_{in}} - T_{AC_{out}}\right) = UA_A \cdot LMTD_A = \dot{m}_r \cdot h_A^v + \dot{m}_{ps} \cdot h_A^{in} - \dot{m}_{rs} \cdot h_A^{out} \quad \text{(eq. 15)}$$

$$Q_G = \dot{m}_G \cdot Cp_w \cdot \left(T_{G_{in}} - T_{G_{out}}\right) = UA_G \cdot LMTD_G = \dot{m}_r \cdot h_G^v + \dot{m}_{ps} \cdot h_G^{out} - \dot{m}_{rs} \cdot h_G^{in} \quad \text{(eq. 16)}$$

$$Q_C = \dot{m}_C \cdot Cp_w \cdot \left(T_{C_{in}} - T_C\right) = UA_C \cdot LMTD_C = \dot{m}_r \cdot (h_G^v - h_C^{out}) \quad \text{(eq. 17)}$$

$$Q_E = \dot{m}_E \cdot Cp_w \cdot \left(T_{E_{in}} - T_E\right) = UA_E \cdot LMTD_E = \dot{m}_r \cdot \left(h_E^{out} - h_E^{in}\right) \quad \text{(eq. 18)}$$

$$\dot{m}_{ps} = m_r + \dot{m}_{rs} \quad \text{(eq. 19)}$$

$$\dot{m}_r = \dot{m}_{ps}\left(1 - \frac{X_{ps}}{X_{rs}}\right) \quad \text{(eq. 20)}$$

Due to the fact that no phase change occurs in the solution heat exchanger (SHE), it could be described just with the efficiency (eq. 21).

$$\eta_{SHE} = \frac{T_G^{out} - T_{SHE}}{T_G^{out} - T_{pump}} \quad \text{(eq. 21)}$$

The solution pump work can be described by (eq. 22) and the rich solution enthalpy at the outlet of the solution pump can be expressed by (eq. 23).

$$W_{pump} = \frac{\dot{m}_{rs} \cdot dP}{\eta_{pump} \cdot \rho_A^{rs}} \quad \text{(eq. 22)}$$

$$h_{pump} = h_A^{out} + \frac{W_{pump}}{\dot{m}_{rs}} \quad \text{(eq. 23)}$$

Finally, UA_G, UA_A, UA_C, UA_E, η_{SHE} and m_{sp} are the 6 parameters to identify.

[1] Engineering Equation Solver : http://www.fchart.com/ees/

4. Results and discussion

After parameters identification with the first 15 experimental points, the numerical results are compared to experimental ones using the 20 others experimental points available. The figure 2 presents this comparison for COP_{th} and the thermal loads (Q_E, Q_G and Q_{AC}).

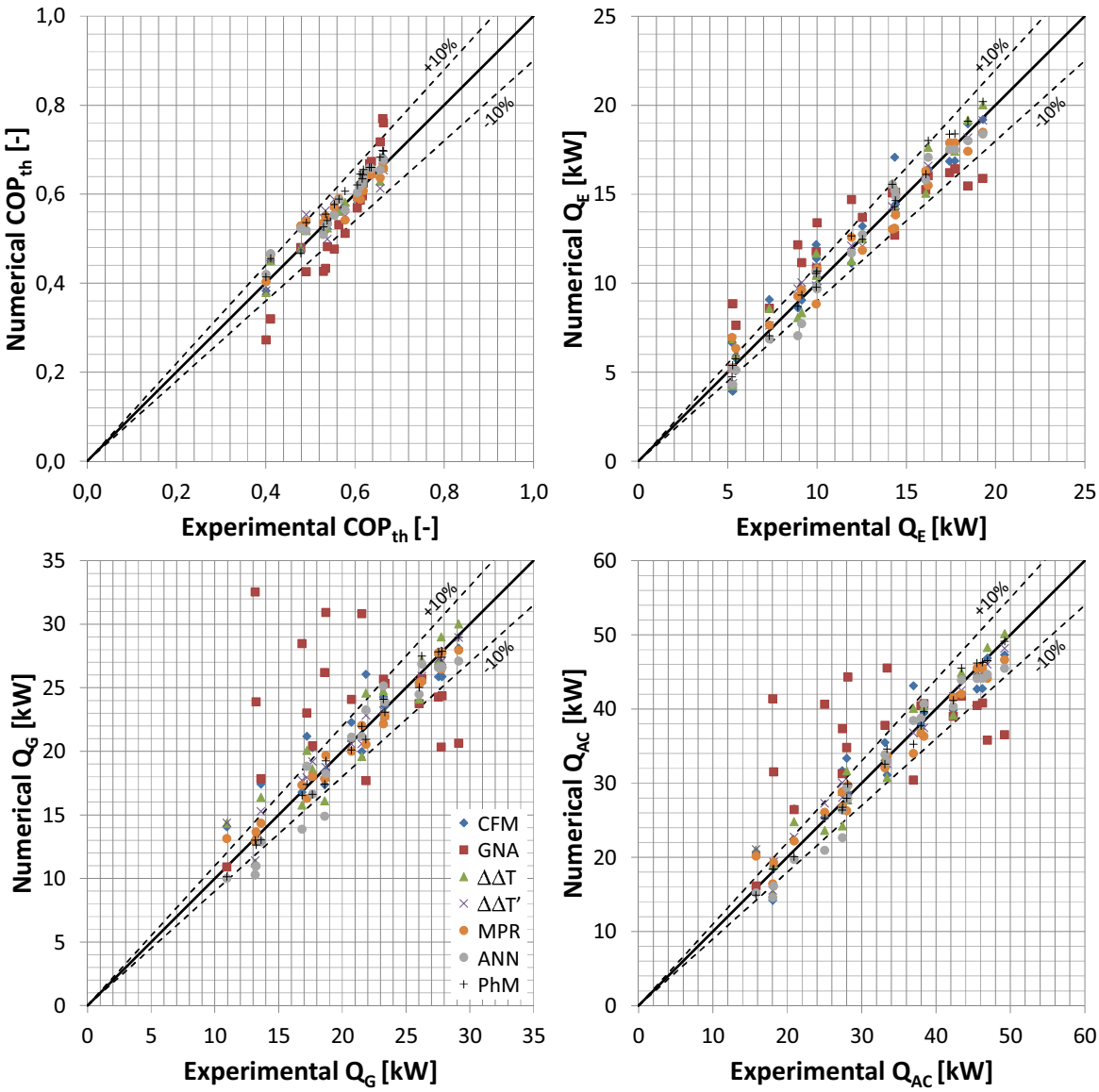

Fig. 2: Comparison between numerical and experimental results for thermal powers (Q_E, Q_{AC} and Q_G) and for the thermal coefficient of performance (COP_{th})

Tab. 2: Coefficient of determination for each model

	CFM	GNA	ΔΔT	ΔΔT'	MPR	ANN	PhM
Q_E	0.943	0.841	0.961	0.984	0.972	0.976	0.991
Q_{AC}	0.909	0.211	0.945	0.978	0.978	0.967	0.991
Q_G	0.851	0.009	0.901	0.963	0.980	0.938	0.989
COP_{th}	0.961	0.913	0.948	0.882	0.911	0.942	0.971

The coefficient of determination (R^2) is used to quantify the quality of the prediction made by each model for both outputs and are presented in Table 2. R^2 can be calculated from the residual sum of squares and the total sum of squares.

Except for the GNA model, the numerical results seem mainly included into a deviation lower than ±10% compared to the experimental results. For Q_E, ΔΔT', ANN and PhM models present the best R^2 values. For

COP_{th}, the best R^2 coefficients are obtained for the CFM, the ΔΔT and PhM models. Considering that it is also important to provide good numerical results for the cooling capacity and for the thermal COP of a chiller, the best compromised can be defined using the figure 3 (left) presenting the relative error on COP_{th} as a function of the relative error of Q_E. The figure 3 (right) shows the value repartitions of the relative errors on COP_{th} and on Q_E on the whole validation points for each numerical model.

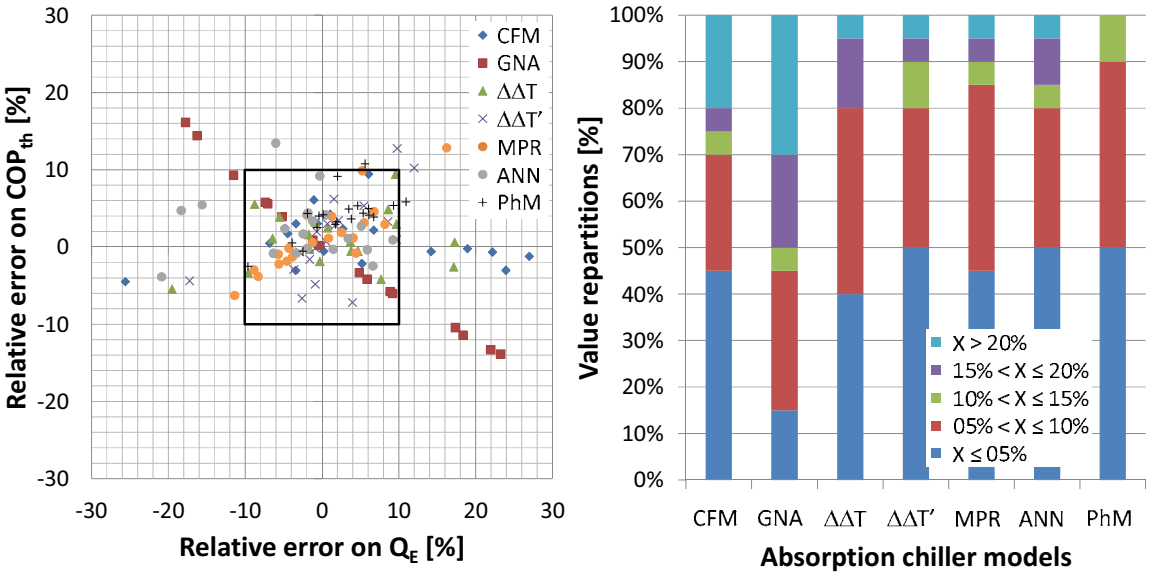

Fig. 3: Comparison of the relative errors on COPth and QE (left) and value repartitions for both on the whole validation points

The numerical results obtained with PhM model presents a global relative error on COP_{th} and Q_E lower than or equal to 15%. ΔΔT, ΔΔT', MPR and ANN models give 80 at 85% of their results with a global relative error on COP_{th} and Q_E lower than or equal to 10%. 80% of the CFM model numerical results have a global relative error lower than or equal to 20%. 30% of the GNA model numerical results have a global relative error upper than 20%.

In order to choose the model to use, an important precision indicator is the number of parameters to determine. In this way, among the empirically based models, the ΔΔT model with 7 parameters (or the ΔΔT' with 8 parameters) is the best choice followed by the CFM model (10 parameters) whereas the ANN and MPR models require respectively 38 and 30 parameters. The PhM model, with only 6 parameters, and a global relative error lower than 15% for the whole validation points seems to be the best choice. But in order to use it, it is necessary to implement physical properties of the solution and of the refrigerant.

5. Conclusions

In this paper, a comparison between the numerical results from different models and the experimental results are presented. The comparison of the 6 empirical models can highlight 3 models with very good results regarding the prediction of the thermal COP and the cooling capacity of the considered chiller. The physical model presents the best results in steady state conditions but needs to implement the physical properties of the working pair. Finally, in order to have numerical results with relative errors on thermal COP and cooling capacity lower than 10%, the characteristic equation model (ΔΔT) (or the adapted characteristic equation model (ΔΔT')) and the Carnot function model (CFM) seems to be interesting solution due to their lower number of parameters. For more accuracy, a physical model could be used.

6. Acknowledgements

Parts of this work have been supported by the AbClimsol and MeGaPICS projects co-financed by the French National Research Agency within the framework of, respectively, the PREBAT and HABISOL programs.

7. Appendix

Tab. 3: Parameters values of the GNA model

α_1	α_2
34,968054	38,120392

Tab. 4: Parameters values of the ΔΔT model

	a_x	b_x
E	0,494804	12,026757
G	0,590091	20,488376
AC	1,0990242	32,429806
R	2,074388	

Tab. 5: Parameters values of the ΔΔT' model

	a'_x	b'_x
E	0,5313756	3,1188152
G	0,6309722	9,9161351
AC	1,1739344	12,762381
R_1	2,5687836	
R_2	2,0191389	

Tab. 6: Parameters values of the MPR model

	E	G	AC
β_0	0,9691217	0,9714067	0,9751444
β_1	-0,207954	-0,1146166	0,0402568
β_2	0,40594	0,4482663	0,5218393
β_3	0,7239341	0,7410667	0,7820739
β_4	0,0020217	-0,0026566	-0,005049
β_5	0,0050033	0,0060896	0,0067634
β_6	-0,0125881	-0,0096777	0,020075
β_7	0,003227	0,0047501	0,0071703
β_8	-0,0202579	-0,019661	-0,0416137
β_9	0,0080407	0,0032297	-0,0033895

Tab. 7: Parameters values of the ANN model

b_1	w_1		
-0,2909412	0,636443	0,9082923	-1,1713704
1,2331352	-5,1690879	2,1492195	1,3085148
-0,4844268	2,4183131	-1,3133123	-1,0843617
-0,3364006	-0,0176307	-1,5496522	-2,1102209
-0,1893325	1,9443634	-2,398689	-1,1833105
0,2954697	1,8799603	0,119088	-2,0443071

b_2	w2					
1,1622436	-1,3393301	2,8714234	-1,1115206	-1,6392393	-1,0345111	-2,0349952
-0,3506204	0,1109996	3,5841658	-2,0677341	-0,6952556	-2,6026828	-1,1316573

Tab. 8: Parameters values of the CFM model

ω_1	τ_1	ω_2	τ_2	$COP_{th,0}$
-0,5642315	1,6053462	-1411,2937	0,1500182	0,6883017
δ_1	θ_1	δ_2	θ_2	$Q_{E,0}$
-275,84153	0,3136397	-28,301388	1,9538139	19,836784

Tab. 9: Parameters values of the PhM model

UA_G [kW/K]	UA_A [kW/K]	UA_C [kW/K]	UA_E [kW/K]	η_{SHE} [-]	m_{sp} [kg/s]
2,6	4,66	5	4	0,7	0,284

8. Nomenclature

8.1. Symbols

b, w	ANN parameters	[-]
COP_{th}	Thermal coefficient of performance	[-]
h	Enthalpy	[J/kg.K]
m	Mass flow rate	[kg/s]
Q	Thermal load	[kW]
R, a_x, b_x	Characteristic temperature function parameters	[-]
R^2	Coefficient of determination	[-]
R_x, a'_x, b'_x	Adapted characteristic temperature function parameters	[-]
T	Temperature	[°C or K]
UA	Global heat transfer coefficient	[W/K]
W	Work	[W]
y, x	Outputs and inputs of ANN model	[-]
ω_x, τ_x, $COP_{th,0}$, δ_x, θ_x, $Q_{E,0}$	CFM parameters	[-]
ΔT_{lm}	Mean differential temperature logarithm	[°C]
$\Delta\Delta T$, $\Delta\Delta T'$	Characteristic and adapted characteristic temperature function	[°C]
α_x	GNA parameters	[-]
β_x	MPR parameters	[-]
η	Efficiency	[-]
φ	Activation function of ANN model	[-]
ρ	Density	[kg/m^3]

8.2. Sub-index

A Absorber

AC absorber/condenser

E	Evaporator
G	Generator
in	Input
out	Output
ps	Poor solution
pump	Solution pump
r	Refrigerant
rs	Rich solution
SHE	Solution heat exchanger
w	water

9. References

Boudéhenn F., Albaric, M., Chatagnon, N, Heinz, J., Benabdelmoumene, N., Papillon P., 2010. Dynamical studies with a semi-virtual testing approach for characterization of small scale absorption chiller. Eurosun Conference, Graz, Austria.

EAW, 2012. Technische Beschreibung, Absorptionskälteanlagen WEGRACAL SE 15. http://www.eaw-energieanlagenbau.de.

Gordon, J.M., Ng, K.C., 1995. A general thermodynamic model for absorption chillers: theory and experiment. Heat recovery Systems and CHP. 15, 73-83

Hernandez J.A., Colorado D., Cortés-Aburto O., El Hamazaoui Y., Velazquez V., Alonso B., 2013. Inverse neural network for optimal performance in polygeneration systems. Applied Thermal Engineering. 50, 1399-1406.

Herold K. E., Radermacher R., Klein S. A., 1996. Absorption chillers and heat pumps. Ed. CRC Press, Taylor & Francis Group, Boca Ranton, United-States.

Kühn, A., Ziegler, F., 2005. Operational results of a 10 kW absorption chiller and adaptation of the characteristic equation. 1st Int. Conf. on Solar Air Conditioning, Bad-Staffelstein, Germany.

Labus, J., Carles Bruno, J., Coronas, A., 2013. Performance analysis of small capacity chillers by using different modeling methods. Applied Thermal Engineering. 58, 305-313

Lansing, F.L., 1976. Computer modeling of a single-stage lithium bromide/water absorption refrigeration unit. The Deep Space Network, p 247-257

Le Denn, A., Boudéhenn, F., Mugnier, D., Papillon P., 2013. A simple predesign tool for solar cooling, heating and domestic hot water production systems. 13th Conference of the Int. Building Performance Simulation Association, Le Bourget du Lac, France.

Schenk H., 2008. Simulation dynamique d'une machine à absorption. Rapport de stage de Polytech'Savoie. 0- 57.

Semmari H., Marc O., Praene J-P., Le Denn J-P., Boudéhenn F., Lucas F., 2014. Sensitivity analysis of the new sizing tool "PISTACHE" for solar heating, cooling and domestic hot water systems. Energy Procedia. 48, 997-1006.

Siré R., Mugnier D., Le Denn A., Morgenstern A., Henning H-M., Boudéhenn F., 2013. Design facilitator: Simplified design tools for solar heating and cooling systems. 4th Int. Conference of Solar Air-Conditioning, Bad Krozingen, Germany.

Ziegler, F., Hellmann, H.M., Schweigler, C., 1999. An approximative method for modeling the operating characteristics of advanced absorption chillers. 29th Int. Congress of Refrigeration, Sydney, Autralia.